SPECIAL FEATURE

On the structure, thermal and tribotechnical properties of the antifriction infiltrated materials based on iron and copper

Larisa Dyachkova [1,*], **Andrey Leonov** [2], **Eugene Feldshtein** [3]

[1] Institute of Powder Metallurgy, Belarusian National Academy of Sciences, Platonova 41, Minsk 220005, Belarus
[2] Belarusian Agrarian Technical University, Nezavisimosty 99, Minsk 220023, Belarus
[3] Department of Mechanical Engineering, University of Zielona Góra, Prof. Z. Szafrana 4, 65-516 Zielona Góra, Poland

This paper describes some properties of the Fe-based materials infiltrated with tin bronze and Cu-based materials infiltrated with tin. It was shown that due to the increased thermal conductivity infiltrated materials based on iron and copper have high tribotechnical properties. With an increase the thermal conductivity the coefficient of friction is reduced, and the seizure pressure increases in infiltrated iron-based materials as a result of the increase in the copper phase and certainty of its morphology, and in copper materials through the creation of a gradient structure in content of tin.

Introduction

There are mechanical, electrical, thermal, vibratory and chemical processes in the friction of machinery. Under the influence of these processes changes occur in the structure of anti-friction material, associated with metal hardening or relaxation, carburization and decarburization, hydrogen saturation or depriving, metal oxidation [1–3]. This can lead to a premature wear of the machine parts. The wear rate depends on many factors, one of which is the material antifriction properties.

According to the molecular–mechanical theory of friction and wear [4] the temperature that develops in the process of friction has the great influence on the performance of the antifriction material. Very high temperatures can arise in the local areas and then in the entire areas of the working surface, which can cause phase transformations in the surface layer and even melting of the material. The high temperature and plastic deformation lead to diffusion processes. As a result of that the coagulation of the individual structural components and the mutual diffusion dissolution of materials of friction pairs are possible [5,6]. To prevent the development of high temperatures in the area of friction, antifriction materials should have high thermal properties, particularly conductivity, a heat capacity and a stable coefficient of the linear thermal expansion. High thermal properties provide a removal and a dissipation of heat generated in the friction zone, protecting the friction units from the excessive heat that can cause decreasing of the mechanical and tribotechnical properties of materials. In addition, the layer of a lubricant can be destroyed that accelerates wear surface oxidation processes, both due to an atmospheric oxygen and oxygen formed due to the decomposition of lubricant decomposition at high temperatures.

Thus, to improve the operability of the antifriction material it should have a high thermal conductivity and a low coefficient of friction. However, with increasing a thermal conductivity, the friction coefficient increases whereas the thermal conductivity of the clean metal is higher than the thermal conductivity of its alloys [7]. However, the alloys have a less ductility, a higher hardness and a strength, thus a high wear resistance and a low friction coefficient.

In our opinion, it can be possible to achieve simultaneous improvements in both parameters through the creation of a composite state. The iron-based materials should include a phase having a significantly higher thermal conductivity, such as copper. The copper materials can create a gradient structure that combines an alloying antifriction layer and a low alloying layer with a high thermal conductivity.

The most effective method for introducing copper into a porous iron skeleton and for the creation of a gradient structure in the copper-based material is the infiltration. This process allows practically eliminating the residual porosity and significant increasing of the strength of the material [8–10].

The driving force of the spontaneous infiltration is a capillary force. Different metal compositions may be infiltrated, such as

Corresponding author. L. Dyachkova (dyachkova@tut.by)

tungsten–cobalt and tungsten–nickel mixtures [11], alumina–steel composites [12], low alloy steels [13]. Copper [11,14] and copper alloys [15,16] are most widely used as infiltrating materials due to their good wetting properties.

The process of the spontaneous infiltration depends on many factors. The study of these factors is the subject of many investigations. In [17] the influence of the shape of the solid phase particles on the infiltration process was studied, in [18] – the impact of the contact angle on the capillary forces, in [19] – the influence of viscosity and capillary forces, in [20–22] – the possibility of the infiltration when components interact. The results of studying infiltration of fusible metals in copper are presented in [23]. It is known that alloying of copper with tin enhances the operational properties by improving the embedability, conformability and resistance to seizure [24,25].

This paper describes the manufacturing process of materials based on iron and copper with a high thermal conductivity and tribotechnical properties that have been produced using the infiltration method.

Experimental procedure

The method for the thermal conductivity testing

The thermal conductivity was measured with the calorimeter using a method of monotonic bilayer plate heating samples 15 mm in diameter and 30 mm in height.

The thermal conductivity was calculated by the equation

$$\lambda(t) = \frac{C_{Ceffect}(t) + 0.5C_O(t) \times h}{(\tau_{HB} - \tau_0) \times S}(1 - \sigma_\alpha - \sigma_k - \sigma_c - \sigma_\lambda),\tag{1}$$

where C_O – sample heat capacity, $C_{Ceffect}$ – effective heat capacity of standard material (AISI 316 steel with thermal conductivity of 13.45 W/(m K)), τ_{HB}, τ_0, σ_α, σ_k, σ_c, σ_λ – coefficients accounted not identical thermocouples, the difference of the standard and sample heating rates and so on.

The heat capacity was calculated by the equation

$$C_x = C_O m_O \times \frac{Q_1}{Q_2},\tag{2}$$

where m_O – the sample mass, Q_1 and Q_2 – the heat flow measured using heat flux sensors.

The thermal conductivity of the copper material infiltrated with tin was calculated according the equation [26]:

$$\lambda = \frac{\lambda_1 \times \lambda_2 \times H}{H_1 \times \lambda_2 + H_2 \times \lambda_1},\tag{3}$$

where λ – the thermal conductivity of copper infiltrated material, W/(m K); H – the height of the sample, m; λ_1, λ_2 – the thermal conductivities of the copper layer and the infiltrated with tin layer accordingly, W/(m K); H_1, H_2 – the heights of the copper layer and the infiltrated with tin layer accordingly, m.

Base powders for P/M materials processing

Ready-made powders of iron, copper, graphite and tin were used. The particulates of the atomized iron powder were of the size less than 200 μm. Graphite with particulates of the size less than 20 μm was used as carbon. The particulates of the copper powder were of the size less than 50 μm, and of tin powder less than 30 μm.

Preparation of composite samples

Two composite materials based of iron and copper obtained by infiltration were studied.

The FeGr1Cu17Sn0.7 iron-based composites based of iron were obtained by infiltrating CuSn5 alloy into a skeleton of FeGr1 composition. The mixture of components was prepared in a mixer of a 'drunken barrel' type for 0.5 h. Then the samples of 82–83% density were pressed using a hydraulic press. The samples were sintered or infiltrated in an electric belt furnace in the atmosphere of an endothermic gas at temperatures of 1100 °C for 1 h.

The copper-based composites were obtained by infiltrating Sn into a skeleton of copper that was pressed at a pressure of 400 MPa and sintering in the atmosphere of an endothermic gas at temperatures of 700 °C for 1 h. To obtain the different copper skeleton densities the porogen of 0.3 and 0.5 wt.% were added into the copper. The samples were infiltrated in the atmosphere of an endothermic gas at temperatures of 400–700 °C for 0.5 h.

The samples of the infiltrate (CuSn5 for the iron-based skeleton or Sn for the copper skeleton) were pressed using a hydraulic press to obtain a density of 65–70%.

The contact infiltration process was used to prepare the composite samples. To ensure a right heating of green preforms of both Fe-based and Cu-based materials they were placed above the pellets of the infiltrate in crucibles on the conveyer of the furnace.

Microstructure and SEM examinations

The microstructure of cross sections of the specimens was examined using an MEF-3 optical microscope. Cross sections of iron-based materials were etched in a 4% solution of a picric acid in an ethyl alcohol and cross sections of copper-based materials were etched in a 3% solution of ferric chloride in ethanol.

Surface textures were analyzed using MIRA scanning electron microscope.

Hardness testing

Hardness was determined by the Brinell hardness tester using the ball of 2.5 mm in diameter and the load of 1839 N. Microhardness was measured using a 'Micromet-II' tester with a load of 0.2 N.

Tribotechnical testing

Tribotechnical tests were carried out in conditions of a distributed contact using a MT-2 tester of a 'pin-on-disc' type. Rotating counter-bodies were made of AISI 1045 steel and had a disc form and hardness of 42–45 HRC. They were in contact with the flat surfaces of the three pin samples 10 mm in diameter. Tests were carried out at the sliding speed of 7 m/s in two stages. In the first stage, average coefficients of friction were determined under the load increasing from 10 N until seizure occurred. In the other stage, the wear rates were determined under a stable load equal to 50 N and the test time of 1 h. I-20 industrial oil was used as the lubricant with the flow rate of 8–10 drops per minute. The magnitude of the linear wear was registered using an optimeter with the accuracy of 0.001 mm.

Results and discussion
Thermal conductivity of MMCs

A skeleton composition, morphology and the amount of the copper phase affect the thermal properties of iron-based MMCs obtained with infiltration. Increasing the density of the skeleton from 75 to 85% leads to the reduction in the thermal conductivity from 80–83 to 70–72 W/(m K). A thermal conductivity of MMCs obtained by infiltration of the green skeleton is 4–10 W/(m K) higher than that obtained by infiltration of the sintered skeleton due to the morphology of the copper phase.

The experimental values of the MMC thermal conductivity are equal to 25–40 W/(m K) that is lower than the calculated ones. This is due to the formation of solid solutions of copper and iron, as well as the purity of the copper phase.

A heat capacity of infiltrated MMCs is almost independent of the copper phase content and morphology and is equal to 460–500 J/(kg K).

A thermal conductivity of the specimen that was made of a copper layer of 10 mm thickness and a tin infiltrate of 400–600 μm thickness was calculated by the equation (3) and was equal to 321 W/(m K). It may be noted that a thermal conductivity for bronze is 110 W/(m K) and for copper 401 W/(m K).

Microstructure investigations

Structure studies were conducted immediately after the infiltration, the duration of which was 20–40 s, and after isothermal exposure at the infiltrating temperature. When infiltration occurs filling the interparticle space by capillary force, as a solid solution in the skeleton is formed by isothermal exposure after infiltration by processes of dissolution and diffusion. After the infiltration, the copper phase is preferably located in grain joint regardless infiltration carried out of sintered or green skeleton (Fig. 1a).

After isothermal 5 min exposure no changes in the structure are revealed. After 10 min exposure a copper phase is observed at the grain boundaries in the MMC with a green steel skeleton (Fig. 1b). A penetration of copper along the grain boundaries is due to the dissolution process of a copper in the iron skeleton and the interdiffusion of copper and iron. With an increase in exposure to 20–30 min the thickness of copper phase layers increases (Fig. 1c). An increase in exposure to 60 min has no effect on the morphology of the copper phase, and at over a 120 min exposure a partial separation of iron skeleton grains is observed.

The distribution of copper phases in MMC based of iron after the infiltration and isothermal exposure depends on the initial density of the skeleton and pore diameters. The porous material with a uniform pore sizes, due to the symmetry of impregnation, has more entrapped air than the porous material, in which there are also small and large pores. The thickness of the copper layers in the infiltrated materials also depends on the perfection of the grain boundaries in an iron skeleton. During sintering, diffusion contacts are formed between the iron particles; the recrystallization occurs and more sophisticated grain boundaries with a lower free energy are formed in the iron skeleton. The sintered skeleton has a narrow pore size range. During sintering primarily fine pores disappear, and the rest of them have the relief smoothed
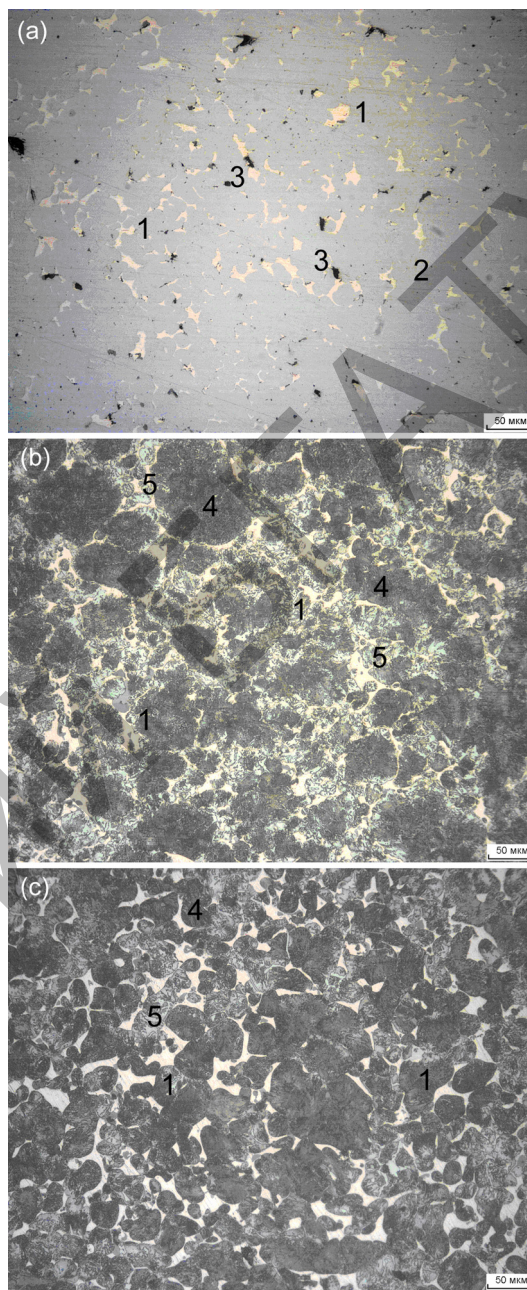
FIGURE 1

The microstructure of the MMCs with green FeGr1 skeleton infiltrated with CuSn5 alloy: **(a)** After infiltration; **(b)** after isothermal exposure 10 min; **(c)** after isothermal holding 60 min: (1) copper phase; (2) iron phase; (3) pore; (4) pearlite; (5) ferrite.

and their specific surface area (a source of high capillary pressure) decreases. Studies have shown that reducing density of the iron-based skeleton from 85 to 75% and increasing average size of the iron powder particles from 70 μm to 150 μm increase the uniformity of distribution of the copper phase, due to an overgrowth of small pores during heating. Therefore green skeleton infiltration is expedient, since there is a wider range of pore sizes.

Because of the processes witch occur during isothermal exposure after infiltration begin earlier for a skeleton area that is in contact with the infiltrate pellets in comparison with the opposite side, the amount of copper of the skeleton varies in
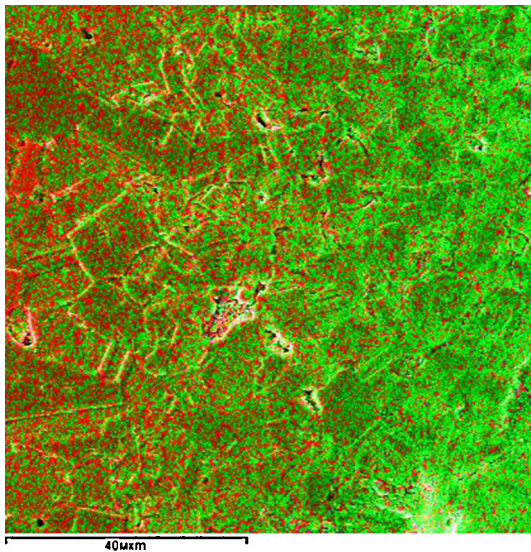
FIGURE 2

The tin (red colour) and copper (green colour) distribution in infiltrated sample of copper.

thickness. The maximum copper content is observed near the contact with the infiltrate pellets, regardless of the original skeleton density.

Similar structural formations are observed during infiltration of tin in the copper skeleton. However, according to the micro X-ray analysis, because of the copper high density tin inclusions are located mainly along the grain boundaries only in the surface region in contact with the tin pellets (Fig. 2).

The porogen addition leads to an increase in the copper skeleton porosity when heated and, respectively, the tin content in the surface layer of the infiltration skeleton increases as well as the tin penetration in the whole volume of the sample.

During isothermal exposure after infiltration the formation of a varying concentration solid solution around the tin inclusions occurs, however large inclusions are not completely dissolved. Solid solution layers are formed around the tin inclusions
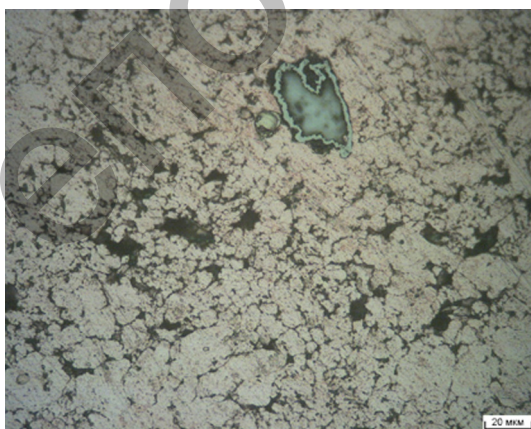

FIGURE 3

Microstructure of copper with 3% porogen infiltrated with tin after isothermal exposure (tin particle has a blue colour).

TABLE 1

The dependence of hardness of infiltrated material on the initial skeleton porosity and carbon content in the skeleton.

The carbon content in the skeleton, %	The initial skeleton porosity, %	Hardness HB
0.4–0.5	22–25	121–129
	13–15	138–140
0.7–0.8	22–25	125–136
	13–15	185–218
1.1–1.2	22–25	130–139
	13–15	185–228
1.8–2.0	22–25	140–170
	13–15	230–240

(Fig. 3), the size of that increases with increasing of the annealing time.

Hardness of the tested materials

The copper phase content and composition of the steel skeleton affect the hardness of infiltrated iron materials (Table 1). With increasing content of copper phase from 15 to 25% the hardness decreases on average by 10–90 HB depending on the carbon content in the skeleton.

The microhardness distribution in the copper infiltrated with tin depends on the porogen content in the skeleton. The microhardness in the near surface zone is equal to 240–255 MPa and at the distance of 250–400 μm is 270–340 MPa.

The hardness of the surface layer in a copper infiltrated tin material increases of more than twice after 1 h isothermal exposure (Fig. 4). Hardening also occurs in the surface area with the porogen additives.

Tribotechnical properties

The friction coefficient of the iron-based material infiltrated with tin bronze is three times lower than that of Cu-10Sn alloy and the seizure pressure is 1.7 times higher. The dependence of the tribotechnical properties on the thermal conductivity is confirmed by the fact that the material obtained by infiltration of the green skeleton has the greater heat conductivity, the seizure pressure is higher and the friction coefficient is lower in comparison with the material obtained by infiltration of the sintered skeleton (Fig. 5).
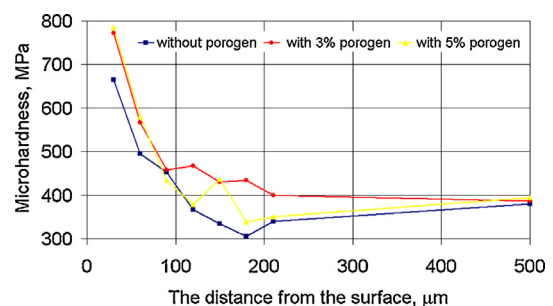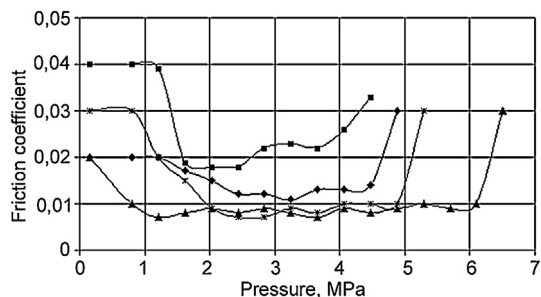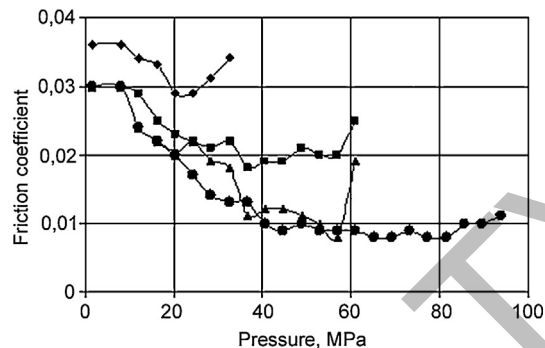

FIGURE 4

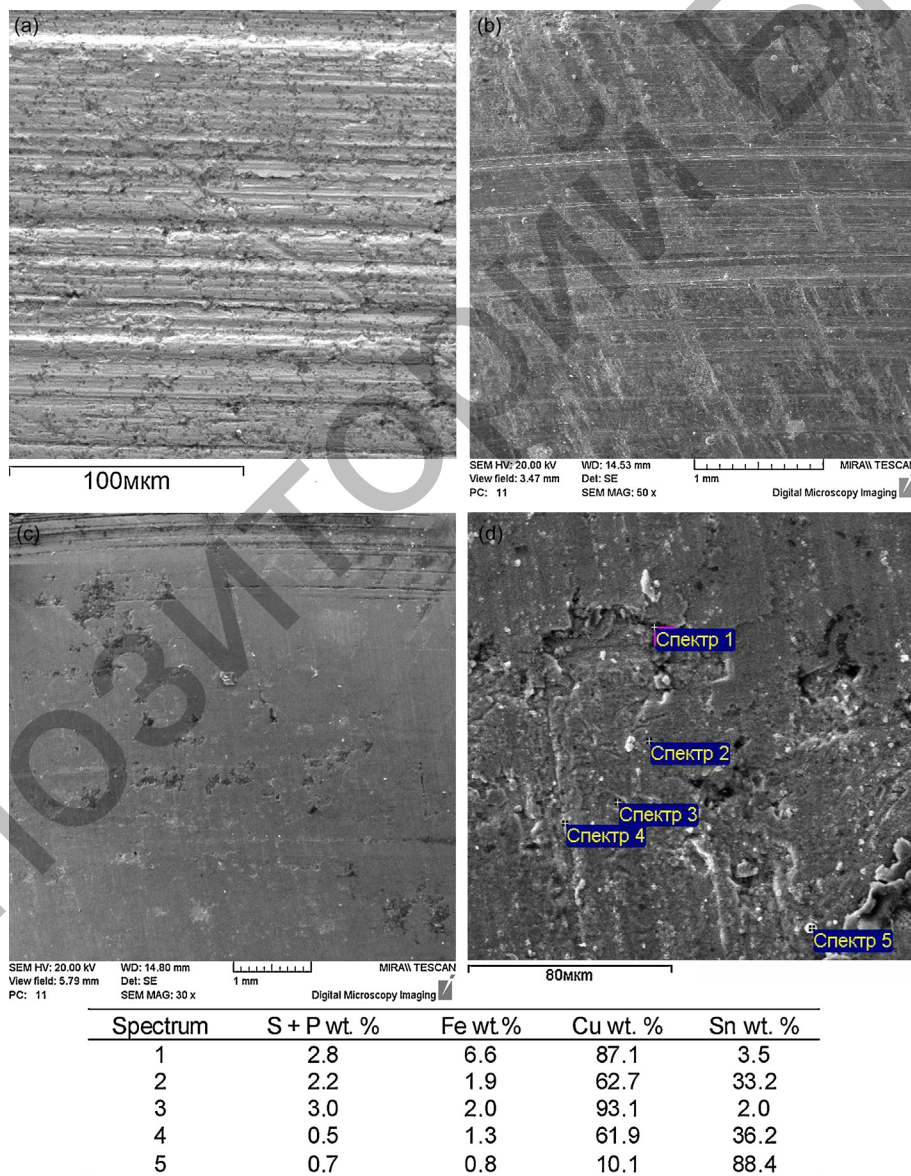Microhadness distribution in copper sample infiltrated with tin after isothermal exposure for 1 h.

FIGURE 5

The effect of pressure on the friction coefficient of infiltrated material with: Fe1Gr sintering skeleton of relative density 75% (×); FeGr1 green skeleton of 75% relative density (); FeGr1 sintering skeleton of 85% relative density (■); FeGr1 green skeleton of 85% relative density (◆) and Cu-10Sn alloy (●).

FIGURE 6

The effect of pressure on the friction coefficient of: CuSn25 sintered material (◆); tin-infiltrated copper (■); tin-infiltrated copper with the addition of 3% porogen (); tin-infiltrated two-layer samples consisting of a copper layer and a copper layer with the addition of 3% porogen (●).

Spectrum	S + P wt. %	Fe wt.%	Cu wt. %	Sn wt. %
1	2.8	6.6	87.1	3.5
2	2.2	1.9	62.7	33.2
3	3.0	2.0	93.1	2.0
4	0.5	1.3	61.9	36.2
5	0.7	0.8	10.1	88.4

FIGURE 7

The morphology of the wear surface of copper powder materials: CuSn25 sintered material **(a)**; tin-infiltrated copper with the addition of 3% porogen **(b)**; tin-infiltrated two-layer material consisting of a copper layer and a copper layer with the addition of 3% porogen **(c)**.

Infiltrated iron-based material also has the higher wear resistance than the sintered material of the same composition due to its high thermal conductivity and strength and uniform distribution of the copper phase. When pressure value is equal 3.5 MPa and speed is equal 4 m/s, the wear rate of infiltrated material FeGr2Cu19Sn0.9 is 13.9×10^{-3} μm/km and the wear rate of the sintered material of the same composition is 59×10^{-3} μm/km.

Tribotechnical tests of the copper-based materials confirmed a great influence of the thermal conductivity and hardness on the friction coefficient and the seizure pressure. The minimal friction coefficient and the maximal seizure pressure were observed for a two-layer tin-infiltrated material (Fig. 6) consisting of a copper layer and a copper layer with the addition of 3% porogen, which has a maximum thermal conductivity. The sintered bronze CuSn25 has the lower tribotechnical properties (Fig. 6). Consequently the wear surface is more rough (Fig. 7). The wear surface of the two-layer infiltrated copper material is smoother (Fig. 7c) when wear surface of tin-infiltrated copper with the addition of 3% porogin (Fig. 7b).

According to the micro X-ray analysis the micro reservoirs formed on the surface during wear process that maintain lubricant (Fig. 7d). The presence of the lubricant is confirmed by the high content of sulfur and phosphorus at were surface.

Conclusions

Tribotechnical properties of infiltrated materials depend on their of thermal conductivity. When thermal conductivity of infiltrated materials increases, the friction coefficient decreases and the seizure pressure increases. Increasing the thermal conductivity of infiltrated iron-based materials by 13–20 W/(m K) is achieved by reduction of an iron skeleton density from 85 to 75%, and using it in an green state. Increasing the thermal conductivity of infiltrated copper-based materials is achieved by creating a gradient structure in tin content, while decreases the size of the infiltrated layer.

The structure of the infiltrated material is formed by infiltration and subsequent isothermal exposure. The distribution of the copper phase by volume iron skeleton depends on the initial density, and the pore diameter, and ideal grain boundaries in the skeleton.

Due to the high green density of the copper skeleton in the infiltrated copper-based material tin inclusions are located only in the surface area in contact with the tin preform. Introduction to 5% porogen provides an increase in the content of tin in the surface layer and its penetration into the whole volume of the skeleton.

The copper phase content and composition of the steel skeleton affect the hardness of infiltrated iron materials. With an increase in content of copper phase from 15 to 25% the hardness decreases on average by 10–90 HB depending on the carbon content in the skeleton. Microhardness distribution in the copper infiltrated with tin material depends on the porogen content in

the skeleton. The microhardness in the near surface zone is equal 240–255 MPa and at the distance of 250–400 μm is 270–340 MPa. Isothermal exposure after infiltration leads to an increase of more than doubles the hardness of the surface layer in a copper material.

Infiltrated iron-based material also has a four times higher wear resistance than the sintered material of the same composition due to its high thermal conductivity and uniform distribution of the copper phase.

Tribotechnical tests of the copper-based materials confirm a great influence of thermal conductivity and hardness on the friction coefficient and the seizure pressure. The minimal friction coefficient and the maximal seizure pressure are obtained for two-layer tin-infiltrated material consisting of a copper layer and a copper layer with the addition of 3% porogen, which has a maximum thermal conductivity.

References

[1] J.F. Archard, in: M.B. Peterson, W.O. Winter (Eds.), Wear Control Handbook, ASME, 1980.
[2] F.P. Bowden, D. Tabor, Friction: An Introduction to Tribology, Anchor Press (The Science Study Series), 1973.
[3] K. Kato, Wear 153 (1992) 277–295.
[4] I.V. Kragelskii, M.N. Dobychin, V.S. Kombalov, Friction and Wear. Calculation Methods, Pergamon Press, Oxford, 1982.
[5] J.P. Hirth, D.A. Rigney, in: P. Haasen et al. (Eds.), Proc. 5th Int. Conf. on Strength of Metals and Alloys, Aachen, Germany, 27–31 August, 1979, Pergamon Press, 1980.
[6] E. Hornbogen, Microstructure and Wear. Metallurgical Aspects of Wear, Deutsche Gesellschaft für Metallkunde, 1981, pp. 23–50.
[7] The Engineering ToolBox, http://www.engineeringtoolbox.com/thermal-conductivity-metals-d_858.html.
[8] P.K. Samal, E. Klar, in: P.W. Lee, Y. Trudel, R. Ronald Iacocca, et al. (Eds.), Powder Metal Technologies and Applications. Vol. 7 of ASM Handbook, ASM International, 1998, pp. 1935–1947.
[9] V.I. Kichigin, O.M. Perel'man, A.I. Rabinovich, N.V. Bezmaternykh, O.P. Koshcheev, Protect. Metal Phys. Chem. Surf. 47 (7) (2011) 921–925.
[10] L.N. Dyachkova, E.E. Feldshtein, J. Mater. Sci. Technol. China 31 (12) (2015) 1226–1231.
[11] M. Ahangarkani, S. Borgi, H. Abbaszadeh, A.A. Rahmani, K. Zangeneh-Madar, Int. J. Refract. Met. Hard Mater. 32 (2012) 39–44.
[12] M. Bahraini, E. Schlenther, J. Kriegesmann, T. Graule, J. Kuebler, Composites: A 41 (2010) 1511–1515.
[13] H. Sanderow, P. Rivest, Mechanical Properties of Copper Infiltrated Low Alloy Steels Using Wrought Wire Infiltrant, http://www.ultrainfiltrant.com/Ultra InfiltratedLowAlloySteels.pdf.
[14] L. Zhang, X.H. Qu, X.B. He, B.H. Duan, S.B. Ren, M.L. Qin, Mater. Sci. Eng. A 489 (2008) 285–293.
[15] Y. Zhu, S. Wang, H. Chen, W. Li, Z. Chen, Ceram. Int. 40 (2014) 2793–2798.
[16] Y. Zhu, S. Wang, H. Chen, W. Li, Z. Chen, Composites: B 56 (2014) 756–761.
[17] H. Mustapha, D.N. Trong, Engineering 3 (2011) 1192–1196.
[18] A. Leger, L. Weber, Acta Mater. 91 (1) (2015) 57–69.
[19] H.E. Dawson, P.V. Roberts, Ground Water 35 (2) (1997) 261–269.
[20] Z. Zhang, S. Long, H.M. Flower, Composites 25 (5) (1994) 380–392.
[21] D. Yi, L. Chuanxi, PM Technol. 8 (3) (1990) 130–135.
[22] A.M. Tartakovsky, A.L. Ward, P. Meakin, Phys. Fluids (2007) 19. Article ID: 103301.
[23] G.A. Libenson, M.J. Lopatin, G.V. Komarnitskiy, Processes of Powder Metallurgy, Moscow, 2002.
[24] A. Zeren, Mater. Des. 28 (8) (2007) 2344–2350.
[25] H. Kato, M. Takama, Y. Iwai, K. Washida, Y. Sasaki, Wear 255 (2003) 573–578.
[26] V.A. Kochetkov, Mech. Compos. Mater. 31 (July (4)) (1996) 337–345.